Available online at www.sciencedirect.com
SCIENCE DIRECT®
Journal of Sound and Vibration 281 (2005) 509–535
JOURNAL OF SOUND AND VIBRATION
www.elsevier.com/locate/jsvi

Nonlinear vibrations of circular cylindrical panels

M. Amabili*

Dipartimento di Ingegneria Industriale, Università di Parma, Parco Area delle Scienze 181/A, 43100 Parma, Italy

Received 15 September 2003; accepted 27 January 2004
Available online 2 October 2004

Abstract

Large-amplitude (geometrically nonlinear) vibrations of circular cylindrical panels with rectangular base, simply supported at the four edges and subjected to radial harmonic excitation in the spectral neighbourhood of the lowest resonances are investigated. Two different nonlinear strain–displacement relationships, from the Donnell's and Novozhilov's shell theories, are used to calculate the elastic strain energy. In-plane inertia and geometric imperfections are taken into account. The solution is obtained by Lagrangian approach. The nonlinear equations of motion are studied by using (i) a code based on arclength continuation method that allows bifurcation analysis and (ii) direct time integration. Numerical results are compared to those available in the literature and convergence of the solution is shown. Interaction of modes having integer ratio among their natural frequencies, giving rise to internal resonances, is also discussed.

1. Introduction

A full literature review of work on the nonlinear vibrations of curved panels and shells is given by Amabili and Païdoussis [1]. Pioneers in the study of large-amplitude vibrations of simply supported, circular cylindrical shallow-shells were Reissner [2], Grigolyuk [3] and Cummings [4]. Leissa and Kadi [5] studied linear and nonlinear free vibrations of shallow doubly curved panels, simply supported at the four edges without in-plane restraints. Donnell's nonlinear shallow-shell

*Tel.: +39-0521-905896; fax: +39-0521-905705.
E-mail address: marco@me.unipr.it (M. Amabili).
*URL:*http://me.unipr.it/mam/amabili/amabili.html.

0022-460X/$ - see front matter © 2004 Elsevier Ltd. All rights reserved.
doi:10.1016/j.jsv.2004.01.021

theory was used in a slightly modified version to take into account the meridional curvature. A single mode expansion of the transverse displacement was used.

Vol'mir et al. [6] studied nonlinear oscillations of simply supported, circular cylindrical panels and plates subjected to an initial deviation from the equilibrium position (response of the panel to initial conditions) by using Donnell's nonlinear shallow-shell theory. Results were calculated by numerical integration of the equations of motion obtained by Galerkin projection, retaining three or five modes in the expansion. The results reported do not show the trend of nonlinearity but only the time response.

Hui [7] studied the influence of imperfections on free vibrations of simply supported circular cylindrical panels; he used Donnell's nonlinear shallow-shell theory and a single-mode expansion; the imperfection was assumed to have the same shape of the single mode used. These imperfections changed the linear vibration frequency (increase or decrease according with the number of circumferential half-waves) and influenced the nonlinearity of the panel. Librescu and Chang [8] investigated geometrically imperfect, doubly curved, undamped, laminated composite panels. The nonlinear theory of shear-deformable shallow panels was used. The nonlinearity was due to finite deformations of the panel due to in-plane loads and imperfections. Only small-amplitude free vibrations superimposed to this finite initial deformation were studied. A single mode was used to describe the free vibrations and the initial imperfections. Imperfections of the panels, of the same shape as the mode investigated, lowered the vibration frequency significantly. Librescu and Chang [8] also described accurately the post-buckling stability. In fact, curved panels are characterized by an unstable post-buckling behaviour, in the sense that they are subject to a snap-through-type instability.

Chia [9] investigated doubly curved panels with rectangular base by using Donnell's nonlinear shallow-shell theory and a single-mode expansion in all the numerical calculations, for both vibration shape and initial imperfection. Only the backbone curves are given. Fu and Chia [10] studied antisymmetrically laminated angle-ply circular cylindrical panels by using the Timoshenko–Mindlin kinematic hypothesis, which is an extension of Donnell's nonlinear shallow-shell theory. Effects of transverse shear deformation, rotary inertia and geometrical imperfections were included in the analysis; in-plane inertia was neglected. The solution was obtained by the harmonic balance method after Galerkin projection with a multimode approach.

Raouf [11] and Raouf and Palazotto [12] studied the nonlinear free vibrations of curved orthotropic panels. They used Donnell's nonlinear theory of shells along with a combination of the Galerkin method and the Lindstedt–Poincaré perturbation method. A single-mode analysis was carried out. Softening and hardening type results were found for panels simply supported at the four edges depending on the dimensions and the material. In particular, Raouf [11] found that the mode with one half-wave in both longitudinal and circumferential directions of thin circular cylindrical panels displays softening nonlinearity when the ratio between the radius and length (R/L) of the panel is smaller than 1.25 or 1.5, for the orthotropic composite material used, but for R/L not too close to zero. Otherwise panels display a hardening nonlinearity.

Kobayashi and Leissa [13] studied free vibrations of doubly curved thick shallow panels; they used the nonlinear first-order shear deformation theory of shells in order to study thick shells. The rectangular boundaries of the panel were assumed to be simply supported at the four edges. A single mode expansion was used for each of the three displacements and two rotations involved in the theory; in-plane and rotational inertia were neglected. The problem was then reduced to one

of a single degree of freedom (dof) describing the radial displacement. Numerical results were obtained for circular cylindrical, spherical and paraboloidal panels. Except for hyperbolic paraboloid shells, a softening behaviour was found, becoming hardening for vibration amplitudes of the order of the shell thickness. However, increasing the radius of curvature, i.e. approaching a flat plate, the behaviour changed and became hardening. The effect of the shell thickness was also investigated.

Yamaguchi and Nagai [14] studied vibrations of shallow cylindrical panels with a rectangular boundary, simply supported for transverse deflection and with in-plane elastic constraints at the boundary. The shell was excited by an acceleration having a constant value plus a harmonic component. Donnell's nonlinear shallow-shell theory was utilised with the Galerkin projection along with a multimode expansion of flexural displacement. Initial imperfection was taken into account in the theoretical formulation but not in the calculations. The harmonic balance method and direct integration were used. The response of the panel was of the softening type over the whole range of possible stiffness values of the in-plane springs (elastic support), becoming hardening for a vibration amplitude of the order of the shell thickness; in-plane constraints reduce the softening nonlinearity, which turns to hardening for smaller vibration amplitudes. The objective of this study was to investigate regions of chaotic motion; these regions were identified by means of Poincaré maps and Lyapunov exponents. It was found that, when approaching the static instability point (due to the constant acceleration load), chaotic shell behaviour may be observed. Using a similar approach, Yamaguchi and Nagai [15] studied oscillations of a circular cylindrical panel, simply supported at the four edges, having an elastic radial spring at the center.

Popov et al. [16] investigated simply supported circular cylindrical panels under an axial harmonic load, giving rise to parametric excitation. Donnell's nonlinear shallow-shell theory was used in conjunction with the Galerkin method with a simple two-mode expansion. An extensive bifurcation and stability analyses were performed.

Free vibrations of doubly curved, laminated, clamped shallow panels, including circular cylindrical panels, were studied by Abe et al. [17]. Both first-order shear deformation theory and classical shell theory (analogous to Donnell's theory) were used. Results obtained neglecting in-plane and rotary inertia are very close to those obtained retaining these effects. Only two modes were considered to interact in the nonlinear analysis for higher modes, while a single mode was used for the mode with one circumferential and one longitudinal half-wave.

Even if many theoretical studies have been published, practically the only experimental results available show significant softening type nonlinearity (for vibration amplitude of about the panel thickness) for thin panels and are reported by Amabili et al. [18].

In the present study, large-amplitude (geometrically nonlinear) vibrations of circular cylindrical panels with rectangular base, simply supported at the four edges and subjected to radial harmonic excitation in the spectral neighbourhood of the lowest resonances are investigated. Two different nonlinear strain–displacement relationships, from the Donnell's and Novozhilov's shell theories, are used to calculate the elastic strain energy. In-plane inertia and geometric imperfections are taken into account. The solution is obtained by Lagrangian approach. The present theory is based on the study developed by Amabili [19] for complete circular cylindrical shells, properly adapted to panels taking into account the different boundary conditions. The nonlinear equations of motion are studied by using (i) a code based on arclength continuation method that allows bifurcation analysis and (ii) direct time integration. Numerical results are compared to those

available in the literature and convergence of the solution is shown. Interaction of modes having integer ratio among their natural frequencies, giving rise to internal resonances, is also discussed.

2. Elastic strain energy of the panel

A circular cylindrical panel with the cylindrical coordinate system $(O; x, r, \theta)$, having the origin O at the centre of one end of the panel, is considered, as shown in Fig. 1. The displacements of an arbitrary point of coordinates (x, θ) on the middle surface of the panel are denoted by u, v and w, in the axial, circumferential and radial directions, respectively; w is taken positive outwards. Initial imperfections of the circular cylindrical panel associated with zero initial tension are denoted by radial displacement w_0, also positive outwards; only radial initial imperfections are considered.

Two different strain–displacement relationships for thin shells are used in the present study, in order to compare results. They are based on Love's first approximation assumptions. These theories are: (i) Donnell's, and (ii) Novozhilov's nonlinear shell theories. According to these two theories, the strain components ε_x, ε_θ and $\gamma_{x\theta}$ at an arbitrary point of the panel are related to the middle surface strains $\varepsilon_{x,0}$, $\varepsilon_{\theta,0}$ and $\gamma_{x\theta,0}$ and to the changes in the curvature and torsion of the middle surface k_x, k_θ and $k_{x\theta}$ by the following three relationships:

$$\varepsilon_x = \varepsilon_{x,0} + zk_x, \quad \varepsilon_\theta = \varepsilon_{\theta,0} + zk_\theta, \quad \gamma_{x\theta} = \gamma_{x\theta,0} + zk_{x\theta}, \tag{1}$$

where z is the distance of the arbitrary point of the panel from the middle surface. The middle surface strain–displacement relationships and changes in the curvature and torsion have different expressions for the Donnell's and Novozhilov's theories.

According to Donnell's nonlinear shell theory, the middle surface strain–displacement relationships and changes in the curvature and torsion for a circular cylindrical panel are [20]

$$\varepsilon_{x,0} = \frac{\partial u}{\partial x} + \frac{1}{2}\left(\frac{\partial w}{\partial x}\right)^2 + \frac{\partial w}{\partial x}\frac{\partial w_0}{\partial x}, \tag{2a}$$

$$\varepsilon_{\theta,0} = \frac{\partial v}{R\partial\theta} + \frac{w}{R} + \frac{1}{2}\left(\frac{\partial w}{R\partial\theta}\right)^2 + \frac{\partial w}{R\partial\theta}\frac{\partial w_0}{R\partial\theta}, \tag{2b}$$

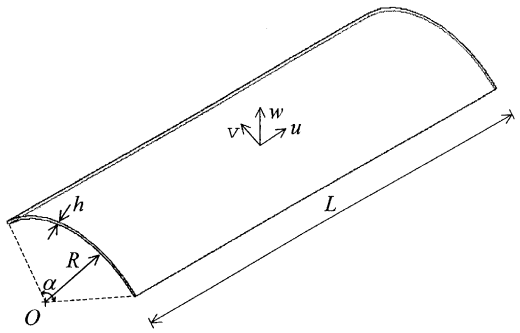

Fig. 1. Geometry of the circular cylindrical panel and coordinate system.

$$\gamma_{x\theta,0} = \frac{\partial u}{R\partial\theta} + \frac{\partial v}{\partial x} + \frac{\partial w}{\partial x}\frac{\partial w}{R\partial\theta} + \frac{\partial w}{\partial x}\frac{\partial w_0}{R\partial\theta} + \frac{\partial w_0}{\partial x}\frac{\partial w}{R\partial\theta}, \tag{2c}$$

$$k_x = -\frac{\partial^2 w}{\partial x^2}, \tag{2d}$$

$$k_\theta = -\frac{\partial^2 w}{R^2\partial\theta^2}, \tag{2e}$$

$$k_{x\theta} = -2\frac{\partial^2 w}{R\partial x\partial\theta}. \tag{2f}$$

According to Novozhilov's nonlinear theory, displacements $\tilde{u}$, $\tilde{v}$ and $\tilde{w}$ of points at distance z from the middle surface are introduced; they are related to displacements on the middle surface by the relationships [20] (it must be observed that Eqs. (8f) and (9a–c) in Ref. [19] present some typing errors corrected here):

$$\tilde{u} = u + z\theta, \tag{3a}$$

$$\tilde{v} = v + z\psi, \tag{3b}$$

$$\tilde{w} = w + w_0 + z\chi, \tag{3c}$$

where

$$\theta = -\frac{\partial(w+w_0)}{\partial x}\left(1 + \frac{\partial v}{R\partial\theta} + \frac{w}{R}\right) + \left(\frac{\partial(w+w_0)}{R\partial\theta} - \frac{v}{R}\right)\frac{\partial u}{R\partial\theta} - \frac{\partial w}{\partial x}\frac{w_0}{R}, \tag{3d}$$

$$\psi = -\left(\frac{\partial(w+w_0)}{R\partial\theta} - \frac{v}{R}\right)\left(1 + \frac{\partial u}{\partial x}\right) + \frac{\partial(w+w_0)}{\partial x}\frac{\partial v}{\partial x}, \tag{3e}$$

$$\chi \cong \frac{\partial u}{\partial x} + \frac{\partial v}{R\partial\theta} + \frac{w+w_0}{R} + \frac{\partial u}{\partial x}\left(\frac{\partial v}{R\partial\theta} + \frac{w+w_0}{R}\right) - \frac{\partial u}{R\partial\theta}\frac{\partial v}{\partial x}. \tag{3f}$$

The strain–displacement relationships for a generic point of the shell are

$$\varepsilon_x = \frac{\partial\tilde{u}}{\partial x} + \frac{1}{2}\left[\left(\frac{\partial\tilde{u}}{\partial x}\right)^2 + \left(\frac{\partial\tilde{v}}{\partial x}\right)^2 + \left(\frac{\partial\tilde{w}}{\partial x}\right)^2\right], \tag{4a}$$

$$\varepsilon_\theta = \frac{1}{R+z}\left(\frac{\partial\tilde{v}}{\partial\theta} + \tilde{w}\right) + \frac{1}{2(R+z)^2}\left[\left(\frac{\partial\tilde{u}}{\partial\theta}\right)^2 + \left(\frac{\partial\tilde{v}}{\partial\theta} + \tilde{w}\right)^2 + \left(\frac{\partial\tilde{w}}{\partial\theta} - \tilde{v}\right)^2\right], \tag{4b}$$

$$\gamma_{x\theta} = \frac{\partial\tilde{v}}{\partial x} + \frac{1}{R+z}\frac{\partial\tilde{u}}{\partial\theta} + \frac{1}{R+z}\left[\frac{\partial\tilde{u}}{\partial x}\frac{\partial\tilde{u}}{\partial\theta} + \frac{\partial\tilde{v}}{\partial x}\left(\frac{\partial\tilde{v}}{\partial\theta} + \tilde{w}\right) + \frac{\partial\tilde{w}}{\partial x}\left(\frac{\partial\tilde{w}}{\partial\theta} - \tilde{v}\right)\right]. \tag{4c}$$

The following thinness approximations are now introduced:

$$1/(R+z) = (1/R)\{1 - z/R + O[(z/R)^2]\}, \tag{5a}$$

$$1/(R+z)^2 = (1/R^2)\{1 - 2z/R + O[(z/R)^2]\}, \tag{5b}$$

where $O((z/R)^2)$ is a small quantity of order $(z/R)^2$. By introducing Eqs. (3) into Eqs. (4) and using approximations (5), the middle surface strain–displacement relationships, changes in the curvature and torsion are obtained for the Novozhilov theory of shells

$$\varepsilon_{x,0} = \frac{\partial u}{\partial x} + \frac{1}{2}\left[\left(\frac{\partial u}{\partial x}\right)^2 + \left(\frac{\partial v}{\partial x}\right)^2 + \left(\frac{\partial w}{\partial x}\right)^2\right] + \frac{\partial w}{\partial x}\frac{\partial w_0}{\partial x}, \tag{6a}$$

$$\begin{aligned}\varepsilon_{\theta,0} = {} & \frac{\partial v}{R\partial\theta} + \frac{w}{R} + \frac{1}{2R^2}\left[\left(\frac{\partial u}{\partial\theta}\right)^2 + \left(\frac{\partial v}{\partial\theta} + w\right)^2 + \left(\frac{\partial w}{\partial\theta} - v\right)^2\right] \\ & + \frac{1}{R^2}\left[\frac{\partial w_0}{\partial\theta}\left(\frac{\partial w}{\partial\theta} - v\right) + w_0\left(w + \frac{\partial v}{\partial\theta}\right)\right],\end{aligned} \tag{6b}$$

$$\begin{aligned}\gamma_{x\theta,0} = {} & \frac{\partial v}{\partial x} + \frac{\partial u}{R\partial\theta} + \frac{1}{R}\left[\frac{\partial u}{\partial x}\frac{\partial u}{\partial\theta} + \frac{\partial v}{\partial x}\left(\frac{\partial v}{\partial\theta} + w\right)\right. \\ & \left. + \frac{\partial w}{\partial x}\left(\frac{\partial w}{\partial\theta} - v\right) + \frac{\partial w_0}{\partial x}\left(\frac{\partial w}{\partial\theta} - v\right) + \frac{\partial w}{\partial x}\frac{\partial w_0}{\partial\theta} + \frac{\partial v}{\partial x}w_0\right],\end{aligned} \tag{6c}$$

$$\begin{aligned}k_x = {} & -\frac{\partial^2 w}{\partial x^2} + \frac{\partial v}{R\partial x}\left(-\frac{\partial u}{R\partial\theta} + \frac{\partial v}{\partial x} - \frac{\partial^2(w+w_0)}{\partial x\partial\theta}\right) + \frac{\partial(w+w_0)}{\partial x}\frac{\partial^2 u}{\partial x^2} \\ & + \frac{\partial^2 u}{R\partial x\partial\theta}\left(-\frac{v}{R} + \frac{\partial(w+w_0)}{R\partial\theta}\right) + \frac{\partial^2(w+w_0)}{R\partial x\partial\theta}\frac{\partial u}{R\partial\theta} \\ & - \frac{\partial^2(w+w_0)}{\partial x^2}\left(\frac{w}{R} + \frac{\partial v}{R\partial\theta} + \frac{\partial u}{\partial x}\right) - \frac{\partial^2 w}{\partial x^2}\frac{w_0}{R},\end{aligned} \tag{6d}$$

$$\begin{aligned}k_\theta = {} & -\frac{\partial^2 w}{R^2\partial\theta^2} + \frac{\partial u}{R\partial x} + \frac{\partial v}{R^2\partial\theta} - \frac{(w+w_0)}{R}\left(\frac{\partial^2 w}{R^2\partial\theta^2} - \frac{\partial v}{R^2\partial\theta} - 2\frac{\partial u}{R\partial x}\right) \\ & - \frac{w}{R}\frac{\partial^2 w_0}{R^2\partial\theta^2} - \frac{\partial u}{R^2\partial\theta}\left(\frac{\partial u}{R\partial\theta} + \frac{\partial v}{\partial x} + \frac{\partial^2(w+w_0)}{\partial x\partial\theta}\right) \\ & + \frac{\partial v}{R^2\partial\theta}\left(\frac{\partial v}{R\partial\theta} + 3\frac{\partial u}{\partial x} - \frac{\partial^2(w+w_0)}{R\partial\theta^2}\right) + \frac{\partial^2 v}{R^3\partial\theta^2}\left(\frac{\partial(w+w_0)}{\partial\theta} - v\right) \\ & + \frac{\partial(w+w_0)}{R^2\partial\theta}\left(-\frac{v}{R} + \frac{\partial w}{R\partial\theta}\right) - \frac{\partial^2(w+w_0)}{R^2\partial\theta^2}\frac{\partial u}{R\partial x} + \frac{\partial w}{R^2\partial\theta}\frac{\partial w_0}{R\partial\theta} \\ & + \frac{\partial(w+w_0)}{\partial x}\frac{\partial^2 v}{R\partial x\partial\theta} + \frac{\partial v}{R\partial x}\frac{\partial^2(w+w_0)}{\partial x\partial\theta},\end{aligned} \tag{6e}$$

$$
\begin{aligned}
k_{x\theta} = & -2\frac{\partial^2 w}{R\partial x\partial\theta} - \frac{\partial u}{R^2\partial\theta} + \frac{\partial v}{R\partial x} + \frac{\partial u}{R^2\partial\theta}\left(-\frac{\partial u}{\partial x} + \frac{\partial^2(w+w_0)}{R\partial\theta^2} - \frac{\partial v}{R\partial\theta}\right) \\
& + \frac{\partial^2(w+w_0)}{\partial x^2}\frac{\partial v}{\partial x} - \frac{v}{R^2}\left(\frac{\partial^2 u}{R\partial\theta^2} + \frac{\partial^2 v}{\partial x\partial\theta} + \frac{\partial(w+w_0)}{\partial x}\right) + \frac{\partial(w+w_0)}{R^2\partial\theta}\left(\frac{\partial^2 u}{R\partial\theta^2} + \frac{\partial w}{\partial x} + \frac{\partial^2 v}{\partial x\partial\theta}\right) + \frac{\partial w}{R^2\partial\theta}\frac{\partial w_0}{\partial x} \\
& + \frac{\partial v}{R\partial x}\left(\frac{w+w_0}{R} + 2\frac{\partial v}{R\partial\theta} - \frac{\partial^2(w+w_0)}{R\partial\theta^2} + 2\frac{\partial u}{\partial x}\right) + \frac{\partial(w+w_0)}{\partial x}\left(\frac{\partial^2 u}{R\partial x\partial\theta} + \frac{\partial^2 v}{\partial x^2}\right) \\
& - 2\frac{\partial^2(w+w_0)}{R\partial x\partial\theta}\left(\frac{w}{R} + \frac{\partial v}{R\partial\theta} + \frac{\partial u}{\partial x}\right) - 2\frac{\partial^2 w}{R^2\partial x\partial\theta}w_0. \qquad (6f)
\end{aligned}
$$

Eqs. (6a–f) are an improved version of Novozhilov's nonlinear shell theory because approximations (5) have been used instead of neglecting terms in z and z^2 at that point of the derivation as done in Ref. [20]. Nonlinearities in changes of curvature and torsion can be neglected in many applications without loss of accuracy.

The elastic strain energy U_S of a circular cylindrical panel, neglecting σ_z as stated by Love's first approximation assumptions, is given by

$$
U_S = \frac{1}{2}\int_0^{\alpha}\int_0^{L}\int_{-h/2}^{h/2}(\sigma_x\varepsilon_x + \sigma_\theta\varepsilon_\theta + \tau_{x\theta}\gamma_{x\theta})\,\mathrm{d}z\,\mathrm{d}x R(1+z/R)\,\mathrm{d}\theta, \qquad (7)
$$

where h is the panel thickness, R is the panel middle radius, L is the panel length, α is the angular dimension of the panel and the stresses σ_x, σ_θ and $\tau_{x\theta}$ are related to the strains for homogeneous and isotropic material ($\sigma_z = 0$, case of plane stress) by

$$
\begin{aligned}
& \sigma_x = \frac{E}{1-v^2}(\varepsilon_x + v\varepsilon_\theta), \quad \sigma_\theta = \frac{E}{1-v^2}(\varepsilon_\theta + v\varepsilon_x), \\
& \tau_{x\theta} = \frac{E}{2(1+v)}\gamma_{x\theta}, \qquad (8)
\end{aligned}
$$

where E is the Young's modulus and v is the Poisson's ratio. By using Eqs. (1,7,8), the following expression is obtained:

$$
\begin{aligned}
U_S = & \frac{1}{2}\frac{Eh}{1-v^2}\int_0^{\alpha}\int_0^{L}\left(\varepsilon_{x,0}^2 + \varepsilon_{\theta,0}^2 + 2v\varepsilon_{x,0}\varepsilon_{\theta,0} + \frac{1-v}{2}\gamma_{x\theta,0}^2\right)\mathrm{d}x R\,\mathrm{d}\theta \\
& + \frac{1}{2}\frac{Eh^3}{12(1-v^2)}\int_0^{\alpha}\int_0^{L}\left(k_x^2 + k_\theta^2 + 2vk_xk_\theta + \frac{1-v}{2}k_{x\theta}^2\right)\mathrm{d}x R\,\mathrm{d}\theta \\
& + \frac{1}{2}\frac{Eh^3}{6R(1-v^2)}\int_0^{\alpha}\int_0^{L}\left(\varepsilon_{x,0}k_x + \varepsilon_{\theta,0}k_\theta + v\varepsilon_{x,0}k_\theta + v\varepsilon_{\theta,0}k_x + \frac{1-v}{2}\gamma_{x\theta,0}k_{x\theta}\right)\mathrm{d}x R\mathrm{d}\theta + O(h^4), \qquad (9)
\end{aligned}
$$

where $O(h^4)$ is a higher-order term in h and the last term in h^3 disappears if z/R is neglected with respect to unity in Eq. (7), as it must be done for Donnell's theory. If this term is neglected, the right-hand side of Eq. (9) can be easily interpreted: the first term is the membrane (also referred to as stretching) energy and the second one is the bending energy. If the last term is retained, membrane and bending energies are coupled.

3. Mode expansion, kinetic energy and external loads

The kinetic energy T_S of a circular cylindrical panel, by neglecting rotary inertia, is given by

$$T_S = \tfrac{1}{2}\rho_S h \int_0^{\alpha}\int_0^{L} (\dot{u}^2 + \dot{v}^2 + \dot{w}^2)\,\mathrm{d}x R\,\mathrm{d}\theta, \tag{10}$$

where ρ_S is the mass density of the panel. In Eq. (10) the overdot denotes a time derivative.

The virtual work W done by the external forces is written as

$$W = \int_0^{\alpha}\int_0^{L} \left(q_x u + q_\theta v + q_r w\right)\,\mathrm{d}x R\,\mathrm{d}\theta, \tag{11}$$

where q_x, q_θ and q_r are the distributed forces per unit area acting in axial, circumferential and radial directions, respectively. Initially, only a single harmonic radial force is considered; therefore $q_x = q_\theta = 0$. The external radial distributed load q_r applied to the panel, due to the radial concentrated force $\tilde{f}$, is given by

$$q_r = \tilde{f}\delta(R\theta - R\tilde{\theta})\delta(x - \tilde{x})\cos(\omega t), \tag{12}$$

where ω is the excitation frequency, t is the time, δ is the Dirac delta function, $\tilde{f}$ gives the radial force amplitude positive in w direction, $\tilde{x}$ and $\tilde{\theta}$ give the axial and angular positions of the point of application of the force, respectively; here, the point excitation is located at $\tilde{x} = L/2$, $\tilde{\theta} = \alpha/2$. Eq. (11) can be rewritten in the following form:

$$W = \tilde{f}\cos(\omega t)(w)_{x=L/2,\theta=\alpha/2}. \tag{13}$$

Eq. (13) specialised for the expression of w used in the present study is given in Section 4, together with the virtual work of axial loads and uniform radial pressure.

In order to reduce the system to finite dimensions, the middle surface displacements u, v and w are expanded by using approximate functions. The classical simply supported boundary conditions at the four panel ends are assumed in this study:

$$v = w = w_0 = N_x = M_x = \partial^2 w_0/\partial x^2 = 0 \quad \text{at } x = 0, L, \tag{14a–f}$$

$$u = w = w_0 = N_\theta = M_\theta = \partial^2 w_0/\partial \theta^2 = 0 \quad \text{at } q = 0,\ \alpha, \tag{15a–f}$$

where N is the normal force and M is the bending moment per unit length.

A base of panel displacements is used to discretise the system. The displacements u, v and w can be expanded by using the following expressions, which satisfy identically the geometric boundary conditions (14a,b, 15a,b):

$$u(x,\theta,t) = \sum_{m=1}^{M}\sum_{n=1}^{N} u_{m,n}(t)\ \sin(n\pi\theta/\alpha)\ \cos(m\pi x/L), \tag{16a}$$

$$v(x,\theta,t)=\sum_{m=1}^{M}\sum_{n=1}^{N}v_{m,n}(t)\ \cos(n\pi\theta/\alpha)\ \sin(m\pi x/L), \tag{16b}$$

$$w(x,\theta,t)=\sum_{m=1}^{M}\sum_{n=1}^{N}w_{m,n}(t)\ \sin(n\pi\theta/\alpha)\ \sin(m\pi x/L), \tag{16c}$$

where n and m are the number of circumferential and longitudinal half-waves, respectively; $u_{m,n}(t)$, $v_{m,n}(t)$ and $w_{m,n}(t)$ are the generalized coordinates that are unknown functions of t. By using a different number of terms in Eqs. (16), it is possible to study the convergence and accuracy of the solution. A sufficiently accurate model for the mode ($m=1$, $n=1$) in case of no internal resonances has been shown to have 9 dofs (for the case studied in Section 5). In particular, the following terms in Eq. (16) have been used: $m=1,3$ and $n=1,3$ in Eqs. (16a,b) and $m=1$ and $n=1$ in Eq. (16c).

3.1. Geometric imperfections

Initial geometric imperfections of the circular cylindrical panel are considered only in radial direction. They are associated with zero initial stress. The radial imperfection w_0 is expanded in the same form of w, i.e. in a double Fourier sine series satisfying the boundary conditions (14c,f, 15c,f) at the panel edges

$$w_0(x,\theta)=\sum_{m=1}^{\tilde{M}}\sum_{n=1}^{\tilde{N}}A_{m,n}\ \sin(n\pi\theta/\alpha)\ \sin(m\pi x/L), \tag{17}$$

where $A_{m,n}$ are the modal amplitudes of imperfections; $\tilde{N}$ and $\tilde{M}$ are integers indicating the number of terms in the expansion.

3.2. Boundary conditions: additional terms in the expansion of in-plane displacements

Eqs. (14) and (15) give the boundary conditions for a simply supported panel. Eqs. (14a–c,f, 15a–c,f) are identically satisfied by the expansions of u, v, w and w_0. On the other hand, Eqs. (14d,e, 15d,e) can be rewritten in the following form [21]:

$$M_x=\frac{Eh^3}{12(1-\nu^2)}(k_x+\nu k_\theta)=0, \tag{18}$$

$$M_\theta=\frac{Eh^3}{12(1-\nu^2)}(k_\theta+\nu k_x)=0, \tag{19}$$

$$N_x=\frac{Eh}{1-\nu^2}\left(\varepsilon_{x,0}+\nu\varepsilon_{\theta,0}\right)=0, \tag{20}$$

$$N_\theta=\frac{Eh}{1-\nu^2}\left(\varepsilon_{\theta,0}+\nu\varepsilon_{x,0}\right)=0. \tag{21}$$

Eqs. (18) and (19) are identically satisfied for the expressions of k_x and k_θ given in Eqs. (2d,e) and (6d,e) for Donnell's and Novozhilov's (in this case, these are exactly satisfied only if nonlinear terms in k_x and k_θ are neglected) nonlinear shell theories, respectively.

Eqs. (20) and (21) are not identically satisfied for both the nonlinear shell theories. According to Donnell's theory, see Eqs. (2a,b), and eliminating null terms at the panel edges, Eqs. (20) and (21) can be rewritten as

$$\left[\frac{\partial\hat{u}}{\partial x}+\frac{1}{2}\left(\frac{\partial w}{\partial x}\right)^2+\frac{\partial w}{\partial x}\frac{\partial w_0}{\partial x}+\frac{v}{R}\frac{\partial\hat{v}}{\partial\theta}\right]_{x=0,L}=0, \tag{22}$$

$$\left[\frac{\partial\hat{v}}{R\partial\theta}+\frac{1}{2}\left(\frac{\partial w}{R\partial\theta}\right)^2+\frac{\partial w}{R\partial\theta}\frac{\partial w_0}{R\partial\theta}+v\frac{\partial\hat{u}}{\partial x}\right]_{\theta=0,\alpha}=0, \tag{23}$$

where $\hat{u}$ and $\hat{v}$ are terms that must be added to the expansion of u and v, given in Eq. (16a,b), in order to satisfy exactly the in-plane boundary conditions $N_x=0$ and $N_\theta=0$. As a consequence that $\hat{u}$ and $\hat{v}$ are second order terms in the panel displacement as shown by Eqs. (22) and (23), they have not been inserted in the second order terms that involve u and v in Eqs. (22) and (23).

Non-trivial calculations give

$$\begin{aligned}\hat{u}(t)=&-\frac{1}{8}\sum_{n=1}^{N}\sum_{m=1}^{M}(m\pi/L)\left\{\sum_{k=1}^{N}\sum_{s=1}^{M}2sw_{m,n}w_{s,k}[\cos[(n-k)\pi\theta/\alpha]\right.\\&-\cos[(n+k)\pi\theta/\alpha]]\sin[(m+s)\pi x/L]/(m+s)\\&\left.-w_{m,n}(t)\sin(n\pi\theta/\alpha)\sum_{j=1}^{\tilde{N}}\sum_{i=1}^{\tilde{M}}\frac{i}{m+i}A_{i,j}\sin(j\pi\theta/\alpha)\sin[(m+i)\pi x/L]\right\},\end{aligned} \tag{24a}$$

$$\begin{aligned}\hat{v}(t)=&-\frac{1}{8}\sum_{n=1}^{N}\sum_{m=1}^{M}(n\pi/(R\alpha))\left\{\sum_{k=1}^{N}\sum_{s=1}^{M}2kw_{m,n}w_{s,k}[\cos[(m-s)\pi x/L]\right.\\&-\cos[(m+s)\pi x/L]]\sin[(n+k)\pi\theta/\alpha]/(n+k)\\&\left.-w_{m,n}(t)\sin(m\pi x/L)\sum_{j=1}^{\tilde{N}}\sum_{i=1}^{\tilde{M}}\frac{j}{n+j}A_{i,j}\sin(i\pi x/L)\sin[(n+j)\pi\theta/\alpha]\right\},\end{aligned} \tag{25a}$$

where the time dependence of $w_{m,n}$ from t has been dropped for simplicity.

A simplified version of Eqs. (24a,25a), that can be used in case of small interaction among mode (m,n) and other modes, is

$$\begin{aligned}\hat{u}(t) = & -\tfrac{1}{8}[a_{m,n}(t)+b_{m,n}(t)\cos(2n\pi\theta/\alpha)]\sin(2m\pi x/L)\\ & -(m\pi/L)w_{m,n}(t)\sin(n\pi\theta/\alpha)\sum_{j=1}^{\tilde{N}}\sum_{i=1}^{\tilde{M}}\frac{i}{m+i}A_{i,j}\\ & \times\sin(j\pi\theta/\alpha)\sin[(m+i)\pi x/L],\end{aligned} \tag{24b}$$

$$\begin{aligned}\hat{v}(t) = & -\frac{1}{8R}[c_{m,n}(t)+d_{m,n}(t)\cos(2m\pi x/L)]\sin(2n\pi\theta/\alpha)\\ & -(1/R)(n\pi/\alpha)w_{m,n}(t)\sin(m\pi x/L)\sum_{j=1}^{\tilde{N}}\sum_{i=1}^{\tilde{M}}\frac{j}{n+j}A_{i,j}\\ & \times\sin(i\pi x/L)\sin[(n+j)\pi\theta/\alpha],\end{aligned} \tag{25b}$$

where

$$a_{m,n}(t)=(m\pi/L)w_{m,n}^2, \tag{26}$$

$$b_{m,n}(t)=-(m\pi/L)w_{m,n}^2, \tag{27}$$

$$c_{m,n}(t)=(n\pi/\alpha)w_{m,n}^2, \tag{28}$$

$$d_{m,n}(t)=-(n\pi/\alpha)w_{m,n}^2. \tag{29}$$

For the Novozhilov's nonlinear shell theory, the approximate Eqs. (24b, 25b) are still correct, but Eqs. (26)–(29) are substituted by

$$a_{m,n}(t)=\frac{m\pi}{L}(w_{m,n}^2+v_{m,n}^2)-\frac{\nu}{8R^2}\frac{L}{m\pi}\left(\frac{n\pi}{\alpha}\right)^2u_{m,n}^2, \tag{30}$$

$$b_{m,n}(t)=-\frac{m\pi}{L}(w_{m,n}^2-v_{m,n}^2)+\frac{\nu}{8R^2}\frac{L}{m\pi}\left(\frac{n\pi}{\alpha}\right)^2u_{m,n}^2+\frac{1}{4}\frac{m\pi}{L}v_{m,n}^2, \tag{31}$$

$$c_{m,n}(t)=\frac{n\pi}{\alpha}(w_{m,n}^2+u_{m,n}^2)+\frac{\alpha}{n\pi}v_{m,n}^2-2w_{m,n}v_{m,n}-\frac{\nu R}{8}\frac{\alpha}{n\pi}\left(\frac{m\pi}{L}\right)^2v_{m,n}^2, \tag{32}$$

$$d_{m,n}(t)=-\frac{n\pi}{\alpha}(w_{m,n}^2-u_{m,n}^2)-\frac{\alpha}{n\pi}v_{m,n}^2+2w_{m,n}v_{m,n}+\frac{\nu R}{8}\frac{\alpha}{n\pi}\left(\frac{m\pi}{L}\right)^2v_{m,n}^2+\frac{1}{4R}\frac{n\pi}{\alpha}u_{m,n}^2. \tag{33}$$

4. Lagrange equations of motion

The non-conservative damping forces are assumed to be of viscous type and are taken into account by using the Rayleigh's dissipation function

$$F = \tfrac{1}{2}c \int_0^{2\pi} \int_0^L (\dot{u}^2 + \dot{v}^2 + \dot{w}^2)\, \mathrm{d}x R\, \mathrm{d}\theta, \tag{34}$$

where c has a different value for each term of the mode expansion. Simple calculations give

$$F = \tfrac{1}{2}(L\alpha/4)R \sum_{n=1}^{N} \sum_{m=1}^{M} c_{m,n}(\dot{u}_{m,n}^2 + \dot{v}_{m,n}^2 + \dot{w}_{m,n}^2). \tag{35}$$

The damping coefficient $c_{m,n}$ is related to modal damping ratio, that can be evaluated from experiments, by $\varsigma_{m,n} = c_{m,n}/(2\mu_{m,n}\omega_{m,n})$, where $\omega_{m,n}$ is the natural circular frequency of mode (m, n) and $\mu_{m,n}$ is the modal mass of this mode, given by $\mu_{m,n} = \rho_S h(\alpha L/4)R$.

The virtual work done by the concentrated radial force $\tilde{f}$, given by Eq. (13), is specialized for the expression of w given in Eq. (16c), is

$$W = \tilde{f}\cos(\omega t)(w)_{x=L/2,\theta=\alpha/2} = \tilde{f}\cos(\omega t)\left[\sum_{i=1}^{\hat{M}} \sum_{j=1}^{\hat{N}} (-1)^{i+1}(-1)^{j+1} w_{2i-1,2j-1}(t)\right] \tag{36}$$

where $\hat{M} = \text{integer part}(M/2+1)$ and $\hat{N} = \text{integer part}(N/2+1)$.

In presence of axial loads and radial pressure acting on the panel, additional virtual work is done by the external forces. Consider a time-dependent axial load $N(t)$, per unit length, applied at both the curved ends of the panel; $N(t)$ is positive in the x direction. In particular $-N(t)$ is applied at $x = 0$ and $N(t)$ is applied at $x = L$. The axial distributed force q_x has the following expression

$$q_x = N(t)[-\delta(x) + \delta(x - L)], \tag{37}$$

where δ is the Dirac delta function. The virtual work done by the axial load is

$$W = \int_0^{\alpha} \int_0^L N(t)[-\delta(x) + \delta(x - L)]u\, \mathrm{d}x R\, \mathrm{d}\theta = -\frac{4\alpha}{\pi} RN(t) \sum_{i=1}^{\hat{M}} \sum_{j=1}^{\hat{N}} u_{2i-1,2j-1}(t)/(2j-1). \tag{38}$$

In case of uniform internal time-varying pressure $p_r(t)$, the radial distributed force q_r is obviously

$$q_r = p_r(t). \tag{39}$$

The virtual work done by radial pressure is

$$W = \int_0^{\alpha} \int_0^L p_r(t) w\, \mathrm{d}x R\, \mathrm{d}\theta = \frac{4\alpha L}{\pi^2} R p_r(t) \sum_{i=1}^{\hat{M}} \sum_{j=1}^{\hat{N}} \frac{w_{2i-1,2j-1}(t)}{(2i-1)(2j-1)}. \tag{40}$$

Eqs. (38) and (40) show that only modes with odd number of axial and circumferential half-waves are directly excited by uniform axial loads and radial pressure.

The following notation is introduced for brevity:

$$\mathbf{q} = \{u_{m,n}, v_{m,n}, w_{m,n}\}^{\mathrm{T}}, \quad m = 1, \ldots, M \text{ and } n = 1, \ldots, N. \tag{41}$$

The generic element of the time-dependent vector $\mathbf{q}$ is referred to as q_j; the dimension of $\mathbf{q}$ is dofs, which is the number of degrees of freedom used in the mode expansion.

The generalized forces Q_j are obtained by differentiation of the Rayleigh's dissipation function and of the virtual work done by external forces

$$Q_j = -\frac{\partial F}{\partial \dot{q}_j} + \frac{\partial W}{\partial q_j} = -(L\alpha/4)Rc_j\dot{q}_j + \begin{cases} 0 & \text{if } q_j = u_{m,n}, v_{m,n}; \text{ or } w_{m,n} \text{ with } m \text{ or } n \text{ even}, \\ \tilde{f}\cos(\omega t) & \text{if } q_j = w_{m,n} \text{ with both } m, n \text{ odd}. \end{cases} \tag{42}$$

The Lagrange equations of motion are

$$\frac{\mathrm{d}}{\mathrm{d}t}\left(\frac{\partial T_S}{\partial \dot{q}_j}\right) - \frac{\partial T_S}{\partial q_j} + \frac{\partial U_S}{\partial q_j} = Q_j, \quad j = 1, \ldots, \text{dofs}, \tag{43}$$

where $\partial T_S/\partial q_j = 0$. These second-order equations have very long expressions containing quadratic and cubic nonlinear terms. In particular,

$$\frac{\mathrm{d}}{\mathrm{d}t}\left(\frac{\partial T_S}{\partial \dot{q}_j}\right) = \rho_S h(\alpha L/4)R\ddot{q}_j, \tag{44}$$

which shows that no inertial coupling among the Lagrange equations exists for the panel with simply supported edges with the mode expansion used.

The very complicated term giving quadratic and cubic nonlinearities can be written in the form

$$\frac{\partial U_S}{\partial q_j} = \sum_{k=1}^{\text{dofs}} q_k f_k + \sum_{i,k=1}^{\text{dofs}} q_i q_k f_{i,k} + \sum_{i,k,l=1}^{\text{dofs}} q_i q_k q_l f_{i,k,l}, \tag{45}$$

where coefficients f have long expressions that include also geometric imperfections.

5. Numerical results

The equations of motion have been obtained by using the *Mathematica* 4 computer software [22] in order to perform analytical surface integrals of trigonometric functions. The generic Lagrange equation j is divided by the modal mass associated with $\ddot{q}_j$ and then is transformed in two first-order equations. A non-dimensionalization of variables is also performed for computational convenience: the frequencies are divided by the natural frequency of the resonant mode; the vibration amplitudes are divided by the panel thickness h. The resulting $2 \times$ dofs equations are studied by using (i) the software AUTO 97 [23] for continuation and bifurcation analysis of nonlinear ordinary differential equations, and (ii) direct integration of the equations of motion by using the DIVPAG routine of the Fortran library IMSL. Continuation methods allow following the solution path, with the advantage that an unstable solution can also be obtained; these are not ordinarily attainable using direct numerical integration. The software AUTO 97 is capable of continuation of the solution, bifurcation analysis and branch switching by using

arclength continuation and collocation methods. In particular, the panel response under harmonic excitation has been studied by using an analysis in two steps: (i) first the excitation frequency has been fixed far enough from resonance and the magnitude of the excitation has been used as bifurcation parameter; the solution has been started at zero force where the solution is the trivial undisturbed configuration of the panel and has been continued up to reach the desired force magnitude; (ii) when the desired magnitude of excitation has been reached, the solution has been continued by using the excitation frequency as bifurcation parameter.

Numerical calculations have been performed for a circular cylindrical panel, simply supported at the four edges, having the following dimension and material properties: length between supports $L = 0.1$ m, radius of curvature $R = 1$ m, thickness $h = 0.001$ m, angular width between supports $\alpha = 0.1$ rad (i.e. the panel has length equal to the circumferential width), Young's modulus $E = 206 \times 10^9$ Pa, mass density $\rho = 7800\,\mathrm{kg/m^3}$ and Poisson ratio $\nu = 0.3$. A panel with the same dimension ratios ($R/L = 10$, $h/L = 0.01$, $R\alpha/L = 1$, $\nu = 0.3$) was previously studied by Kobayashi and Leissa [13]. In all the numerical simulations a modal damping $\varsigma_{1,1} = 0.004$ and a harmonic force excitation $\tilde{f} = 10.68$ N at the centre of the panel have been assumed. Eqs. (24b) and (25b) have been used to evaluate the additional terms necessary to satisfy the in-plane boundary conditions. It must be observed that the additional terms $\hat{u}$ and $\hat{v}$, to be added to the expansion of u and v to satisfy exactly the in-plane boundary conditions, have here a fundamental importance, in contrast with what it has been found for complete shells [19].

5.1. Calculation with Donnell's theory

The natural frequencies of the panel for modes up to six circumferential and three longitudinal half-waves are given in Fig. 2. The natural frequency of the fundamental mode ($m = 1$, $n = 1$) is $\omega_{1,1} = 636.91$ Hz; natural frequencies of other modes used in Eq. (16) are: $\omega_{1,3} = 2444.1$ Hz, $\omega_{3,1} = 2551.3$ Hz and $\omega_{3,3} = 4415.9$ Hz. As a consequence that the studied panel is shallow, the fundamental mode presents only one longitudinal half-wave. For panels with smaller R/L ratio, the fundamental mode can have $n > 1$ circumferential half-waves (but always $m = 1$).

Fig. 3 shows the maximum (in the time period; this is positive, i.e. outwards) of the panel response in radial direction in the spectral neighbourhood of the fundamental mode ($m = 1$, $n = 1$) versus the excitation frequency. Calculations have been performed with two different models; one with 3 and the other with 9 dofs. The model with 3 dofs includes the following terms in Eqs. (16a–c): $w_{1,1}$, $u_{1,1}$, $v_{1,1}$. The model with 9 dofs includes in addition: $u_{3,1}$, $u_{1,3}$, $u_{3,3}$, $v_{1,3}$, $v_{3,1}$, $v_{3,3}$. Results are compared to those obtained by Kobayashi and Leissa [13], where only the backbone curve is given. The present results with 9 dofs are quite close to those in Ref. [13] (considering that the backbone curve, indicating the maximum of the response for different force excitations, approximately passes through the middle of the forced response curve computed in the present calculation) and shows a softening type nonlinearity, turning to hardening for vibration amplitudes larger than the panel thickness. However, present results computed with only 3 dofs are inaccurate, indicating erroneous hardening type nonlinearity. The maximum amplitude (in a time period, outwards) of the most significant generalized coordinates of the 9 dofs model are shown in Fig. 4 with indication of response stability.

In order to check the convergence of the solution, the response has been calculated with a larger model, including 16 dofs. This model has the following additional generalized coordinates with

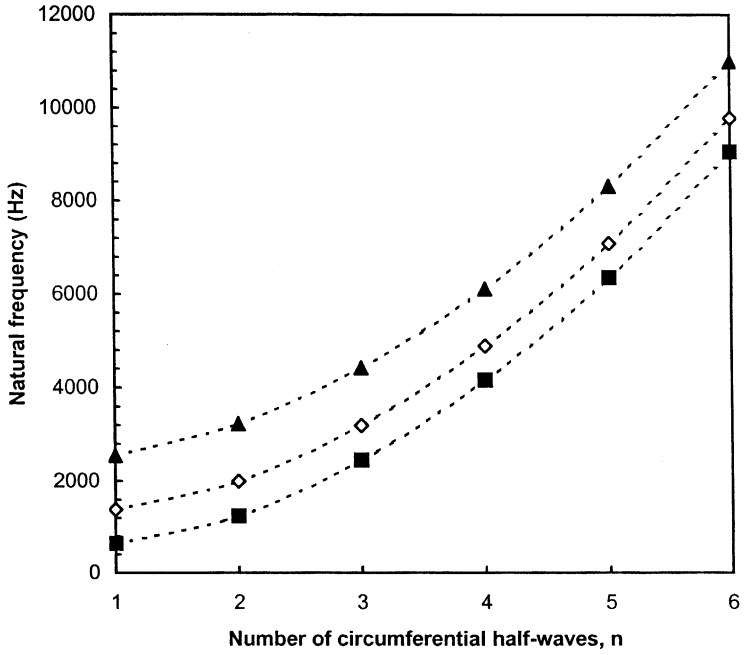

Fig. 2. Natural frequencies of the circular cylindrical panel; Donnell's theory. -■-, $m = 1$; -◇-, $m = 2$; -▲-, $m = 3$.

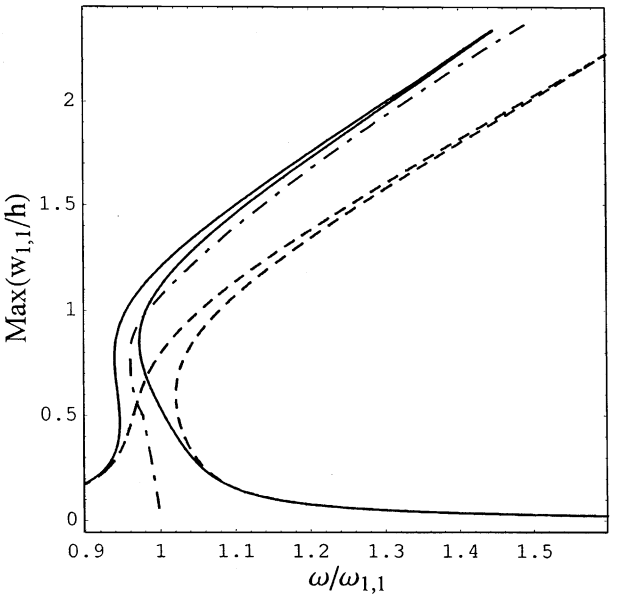

Fig. 3. Maximum amplitude of the radial response of the panel (generalized coordinate $w_{1,1}$) versus the excitation frequency; fundamental mode ($m = 1$, $n = 1$), $\tilde{f} = 10.68$ N and $\zeta_{1,1} = 0.004$; Donnell's theory. —, present results, 9 dofs; - -, present results, 3 dofs; – - –, backbone curve from Kobayashi and Leissa [13].

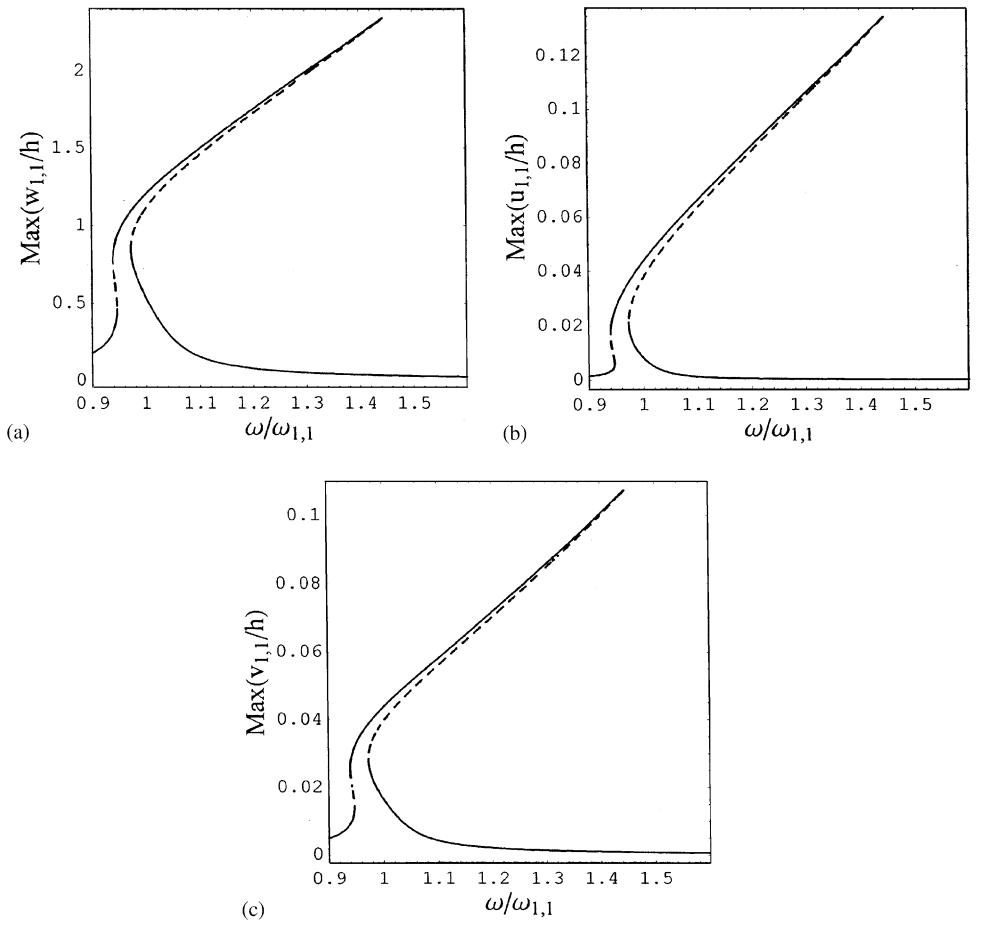

Fig. 4. Maximum amplitude of the response of the panel versus the excitation frequency with stability indication; 9 dofs, fundamental mode ($m = 1, n = 1$), $\tilde{f} = 10.68$ N and $\zeta_{1,1} = 0.004$; Donnell's theory. —, stable solution; - -, unstable solution. (a) Generalized coordinate $w_{1,1}$; (b) $u_{1,1}$; (c) $v_{1,1}$.

respect to the 9 dofs model: $w_{1,3}$, $w_{3,1}$, $w_{3,3}$, $u_{1,5}$, $u_{3,5}$, $v_{1,5}$, v_{35}. Comparison of the response computed with the 16 dofs model to the 9 dofs model and to the backbone curve of Kobayashi and Leissa [13] is presented in Fig. 5. The results of the 16 dofs model are moved slightly to the left with respect to the smaller 9 dofs model, except for a frequency region around $1.25\,\omega_{1,1}$, where there is a quick drop of amplitude of $w_{1,1}$ related to transfer of energy from the generalized coordinate $w_{1,1}$, which is the one in resonance (with in-plane coordinates $u_{1,1}$, $v_{1,1}$, which have smaller amplitudes than $w_{1,1}$), to other generalized coordinates. In fact, at excitation frequency $\omega = 1.279\,\omega_{1,1}$ there is a three-to-one internal resonance due to the relationship $3\,\omega = \omega_{1,3}$, so that the response becomes much more complex. This can be observed in Fig. 6, where the most significant generalized coordinates are shown with indication of response stability. Actually other internal resonances (non-periodic combination resonance [24]) arise in the frequency range shown in Fig. 6: $3(1.223\omega_{1,1}) = 2\omega_{1,3} - \omega_{3,1}$; $3(1.03\omega_{1,1}) = \omega_{3,3} - \omega_{1,3}$; $3(0.98\omega_{1,1}) = \omega_{3,3} - \omega_{3,1}$; as

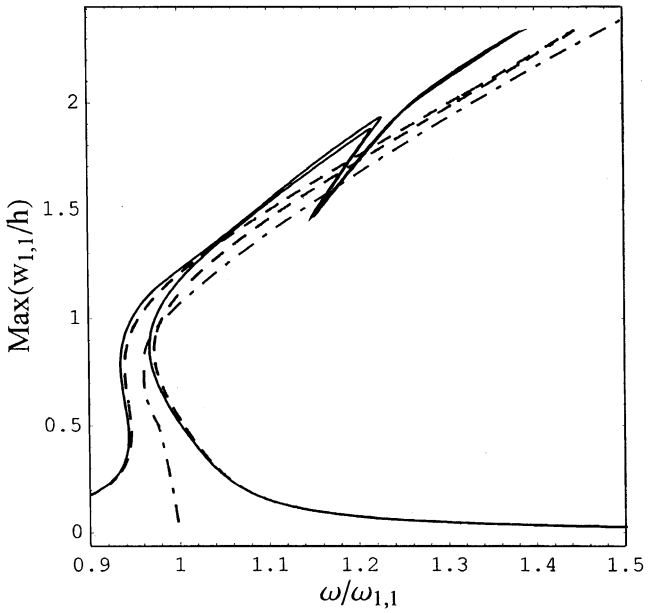

Fig. 5. Maximum amplitude of the radial response of the panel (generalized coordinate $w_{1,1}$) versus the excitation frequency; fundamental mode ($m = 1$, $n = 1$), $\tilde{f} = 10.68$ N and $\zeta_{1,1} = 0.004$; Donnell's theory. —, present results, 16 dofs; - -, present results, 9 dofs; – - –, backbone curve from Kobayashi and Leissa [13].

shown by results, they do not have the same significance. A more accurate study of the internal resonances needs a more refined calculations, reported in Section 5.3.

It is of great importance to analyse the results in the time domain by using direct integration of the equations of motion. Fig. 7 shows the most significant (i.e. those with larger amplitude) generalized coordinates for excitation frequency $\omega = 0.94\,\omega_{1,1}$ (with initial conditions to catch the higher amplitude solution, which is in the softening type region). Results of the generalized coordinates related to radial displacement w clearly indicate that there is a strong asymmetry between vibration inwards and outwards. In fact, the vibration is much larger inwards (negative) than outwards (positive), as previously observed e.g. in Refs. [5,13]; this is related to the curvature of the panel. In particular, for the generalized coordinate $w_{1,1}$, which has the largest amplitude, the inward displacement is 1.5 times bigger than the outward displacement. Moreover, there is a large contribution of higher harmonics, as clearly indicated by the frequency spectra in Fig. 8. In particular, the generalized coordinates $w_{3,1}$, $w_{1,3}$, and $w_{3,3}$ are those more affected by higher harmonics, while $w_{1,1}$ (resonant mode, with $u_{1,1}$ and $v_{1,1}$) is almost perfectly sinusoidal. Phase plane diagrams are also provided in Fig. 9 to better understand the asymmetry of inward and outward vibration; loops are related to higher harmonics.

The same analysis has been performed at excitation frequency $\omega = 1.1\,\omega_{1,1}$ (with initial conditions to catch the higher amplitude solution), where the nonlinear response of the panel turns to hardening type. Results are given in Figs. 10–12, which show an even more significant contribution of higher harmonics. In this case, the inward displacement is 1.7 times bigger than the outward displacement.

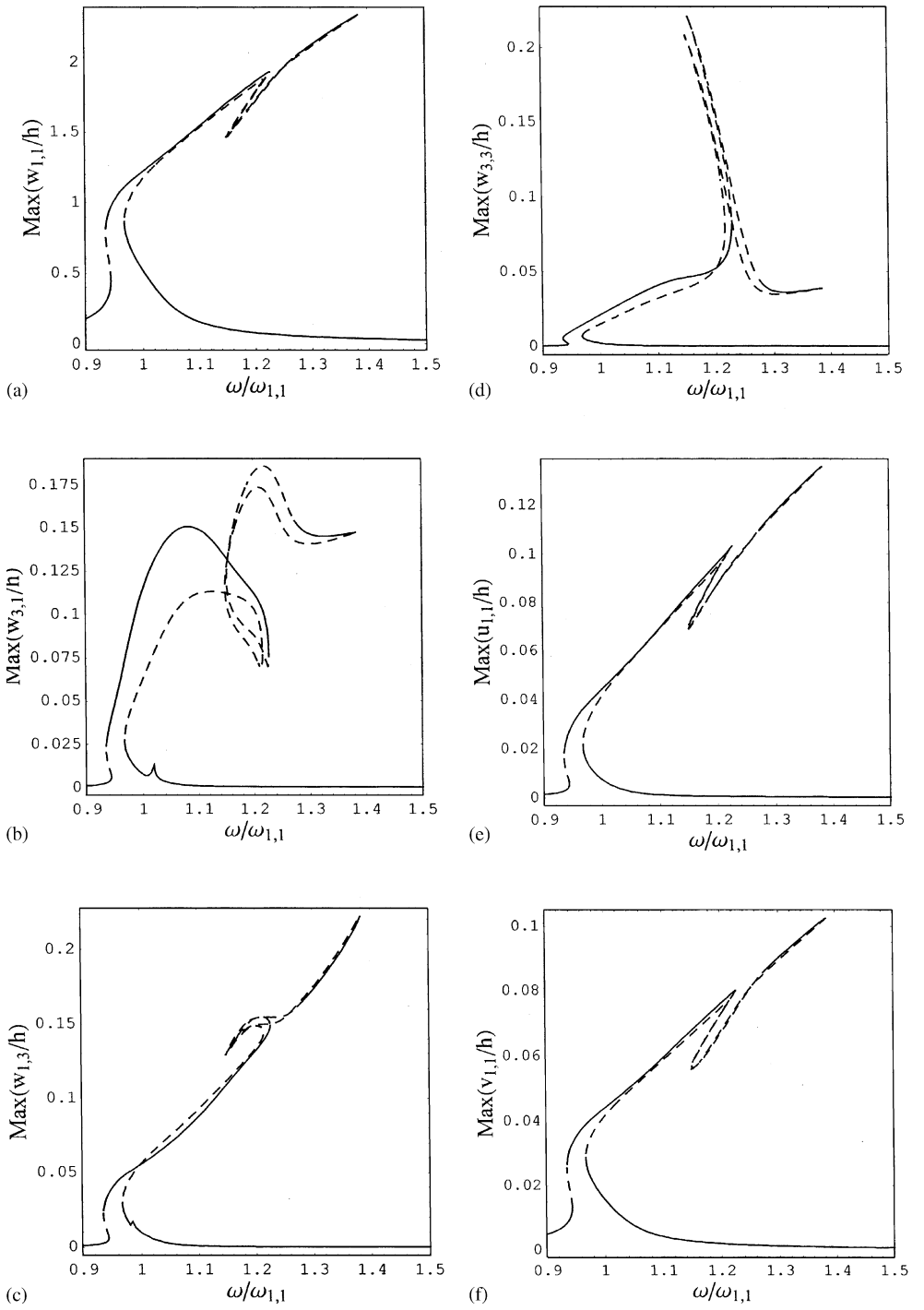

Fig. 6. Maximum amplitude of the response of the panel versus the excitation frequency with stability indication; 16 dofs, fundamental mode ($m = 1, n = 1$), $\tilde{f} = 10.68$ N and $\zeta_{1,1} = 0.004$; Donnell's theory. —, stable solution; - -, unstable solution. (a) Generalized coordinate $w_{1,1}$; (b) $w_{3,1}$; (c) $w_{1,3}$; (d) $w_{3,3}$; (e) $u_{1,1}$; (f) $v_{1,1}$.

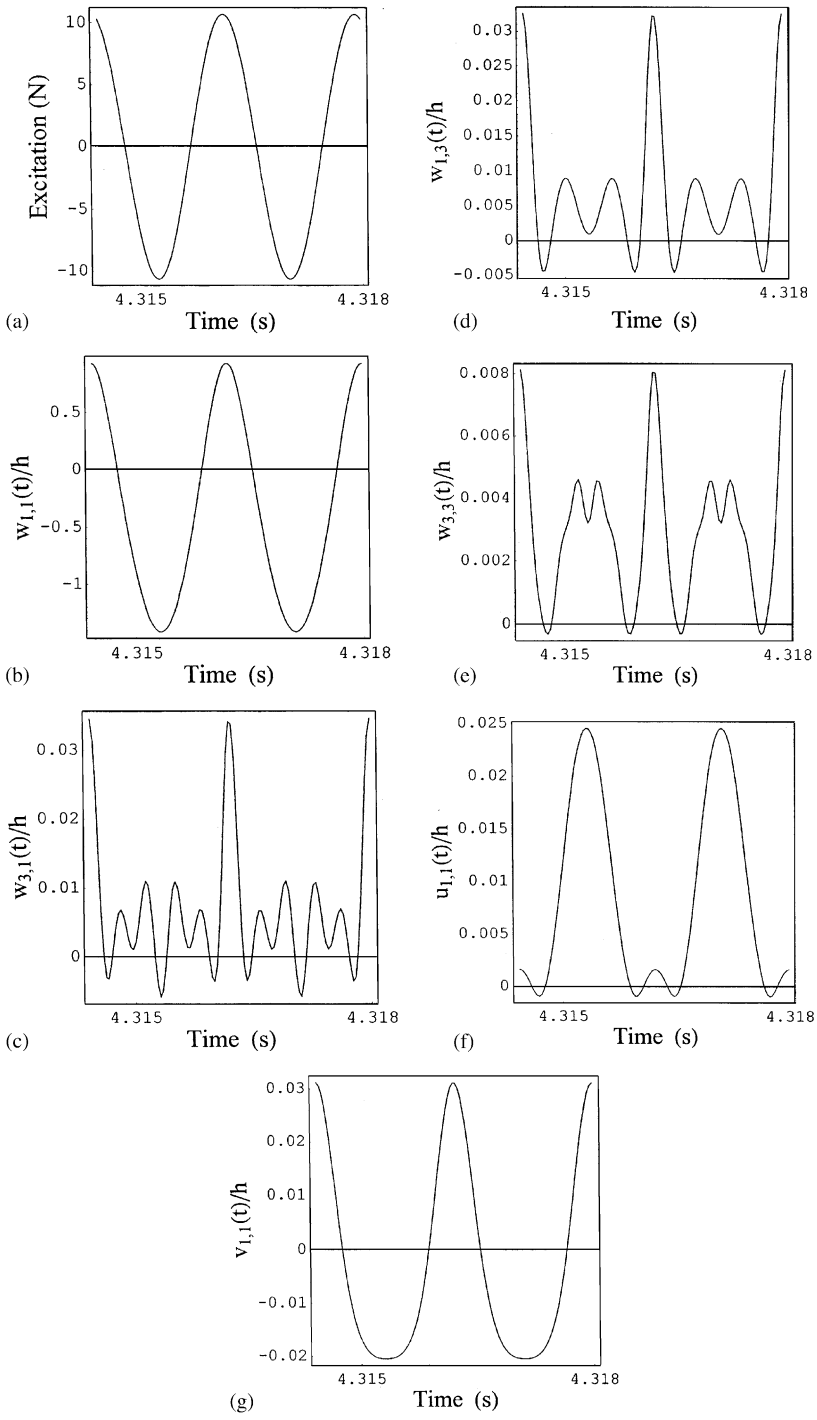

Fig. 7. Time-domain response of the panel; excitation frequency $\omega = 0.94\,\omega_{1,1}$, $\tilde{f} = 10.68$ N and $\zeta_{1,1} = 0.004$; 16 dofs. (a) Excitation; (b) generalized coordinate $w_{1,1}$; (c) generalized coordinate $w_{3,1}$; (d) generalized coordinate $w_{1,3}$; (e) generalized coordinate $w_{3,3}$; (f) generalized coordinate $u_{1,1}$; (g) generalized coordinate $v_{1,1}$.

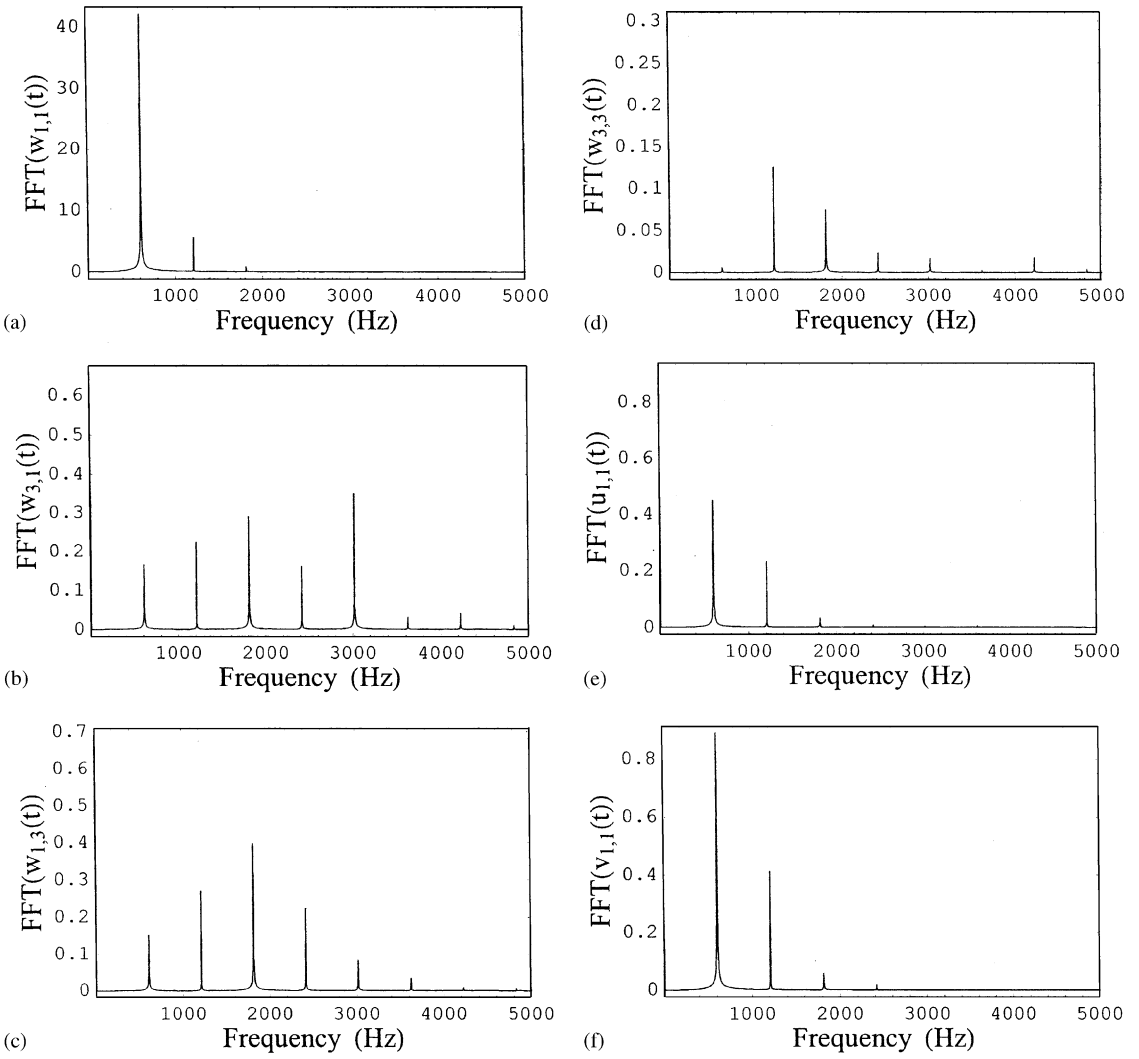

Fig. 8. Spectrum of the response of the panel; excitation frequency $\omega = 0.94\,\omega_{1,1}, \tilde{f} = 10.68$ N and $\zeta_{1,1} = 0.004$; 16 dofs. (a) Generalized coordinate $w_{1,1}$; (b) generalized coordinate $w_{3,1}$; (c) generalized coordinate $w_{1,3}$; (d) generalized coordinate $w_{3,3}$; (e) generalized coordinate $u_{1,1}$; (f) generalized coordinate $v_{1,1}$.

5.2. Calculation with Novozhilov's theory

Comparison of results obtained by using the Novozhilov's and Donnell's nonlinear shell theories is given in Fig. 13. Results are practically coincident in this case ($m = 1$, $n = 1$) and have been computed by using 16 dofs. Natural frequency of mode ($m = 1$, $n = 1$) is $\omega_{1,1}$ =636.76 Hz according to Novozhilov's, which is also practically coincident with Donnell's result. These results indicate that, at least for the thin shallow panel studied here, there is no advantage in using the more refined Novozhilov's shell theory, which is much more time consuming in computation.

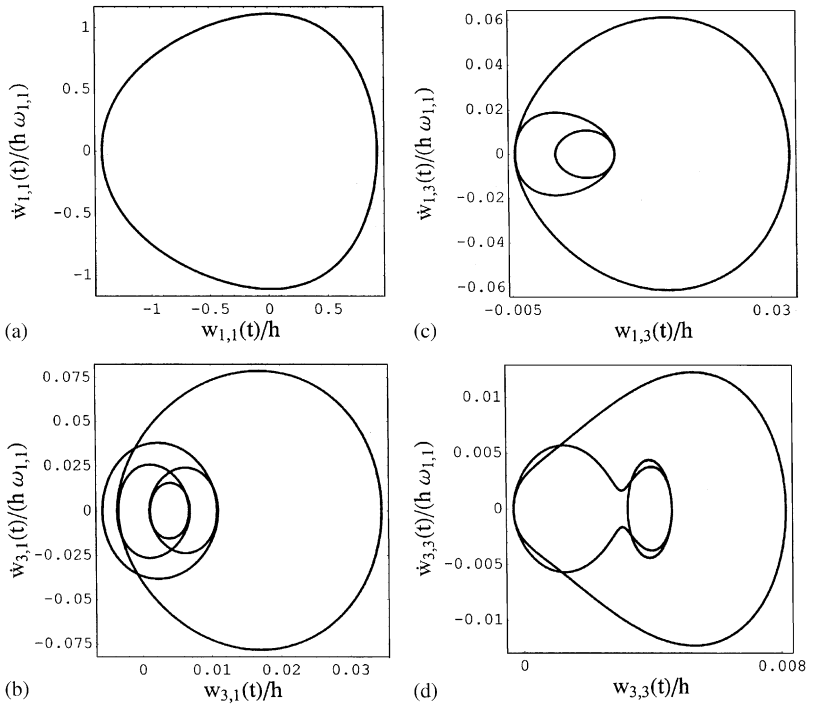

Fig. 9. Phase plane diagram of the panel; excitation frequency $\omega = 0.94\,\omega_{1,1}$, $\tilde{f} = 10.68$ N and $\zeta_{1,1} = 0.004$; 16 dofs. (a) Generalized coordinate $w_{1,1}$; (b) generalized coordinate $w_{3,1}$; (c) generalized coordinate $w_{1,3}$; (d) generalized coordinate $w_{3,3}$.

A similar result has been found for a vibration amplitude of about 5 times the shell thickness of mode ($m = 1$, $n = 1$), which is no more the fundamental mode, of a deeper shell with the same material properties and the following dimensions: $L = 0.4$ m, $R = 1$ m, $h = 0.001$ m, $\alpha = 0.4$ rad. It can be observed that for a circular cylindrical shell complete around the circumference (closed shell), Amabili [19] has shown that significant differences arise between Donnell's and Novozhilov's theories only when in-plane inertia is neglected in Donnell's theory. However, differences between Donnell's and Novozhilov's theories retaining in-plane inertia for complete and deep shells are slightly larger (but still negligible) than in the case of the shallow shell shown in Fig. 13 due to the fact that in these cases larger in-plane displacements arise.

5.3. *Internal resonances with more refined calculations*

Calculations have been performed for the model with 24 dofs and Donnell's theory by using the more accurate Eqs. (24a, 25a) instead of (24b, 25b); the 24 dofs model has the following additional generalized coordinates with respect to the 16 dofs model: $u_{1,7}$, $u_{1,9}$, $u_{3,7}$, $u_{3,9}$, $v_{1,7}$, $v_{1,9}$, $v_{3,7}$, $v_{3,9}$. Results are presented in Figs. 14 and 15 and indicated an even stronger phenomenon of internal resonances. Figs. 14 and 15 can be compared to the analogous Figs. 5 and 6, respectively, which

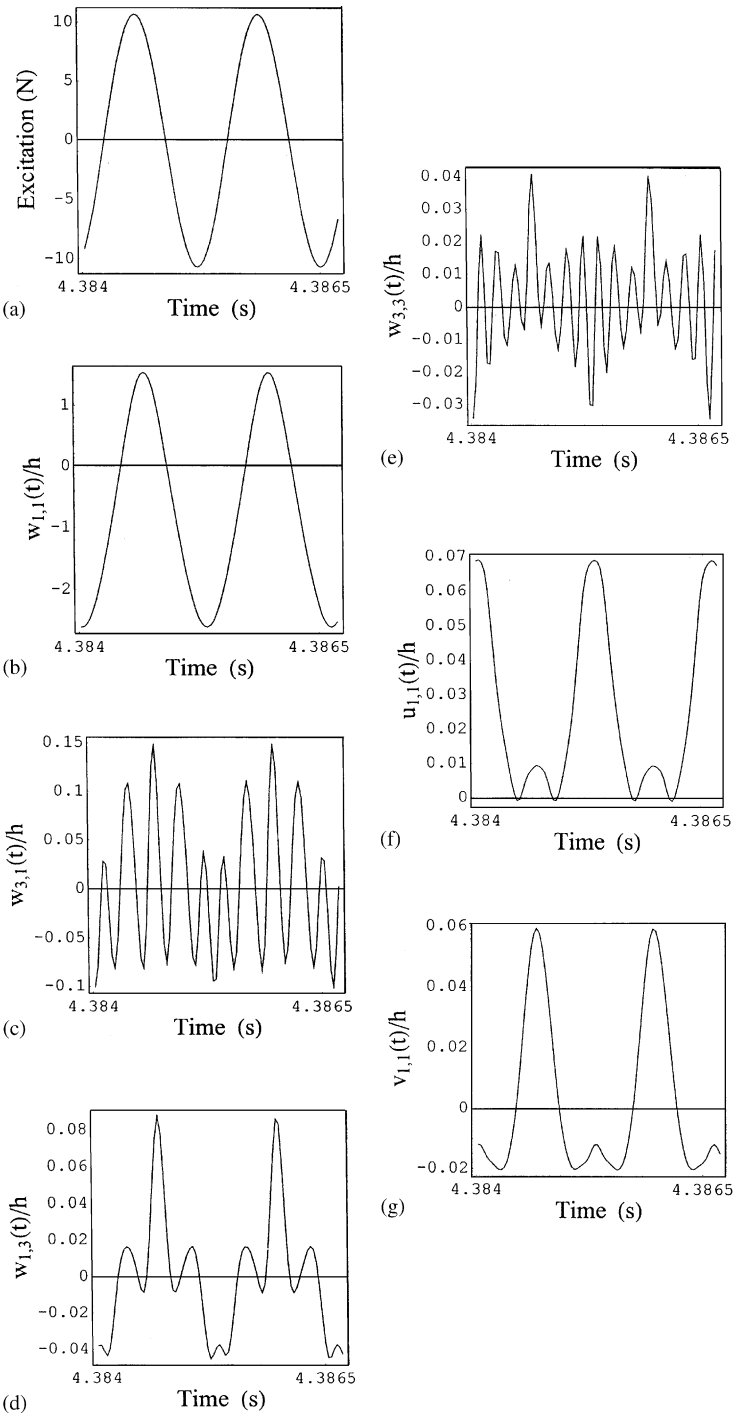

Fig. 10. Time-domain response of the panel; excitation frequency $\omega = 1.1\,\omega_{1,1}$, $\tilde{f} = 10.68$ N and $\zeta_{1,1} = 0.004$; 16 dofs. (a) Excitation; (b) generalized coordinate $w_{1,1}$; (c) generalized coordinate $w_{3,1}$; (d) generalized coordinate $w_{1,3}$; (e) generalized coordinate $w_{3,3}$; (f) generalized coordinate $u_{1,1}$; (g) generalized coordinate $v_{1,1}$.

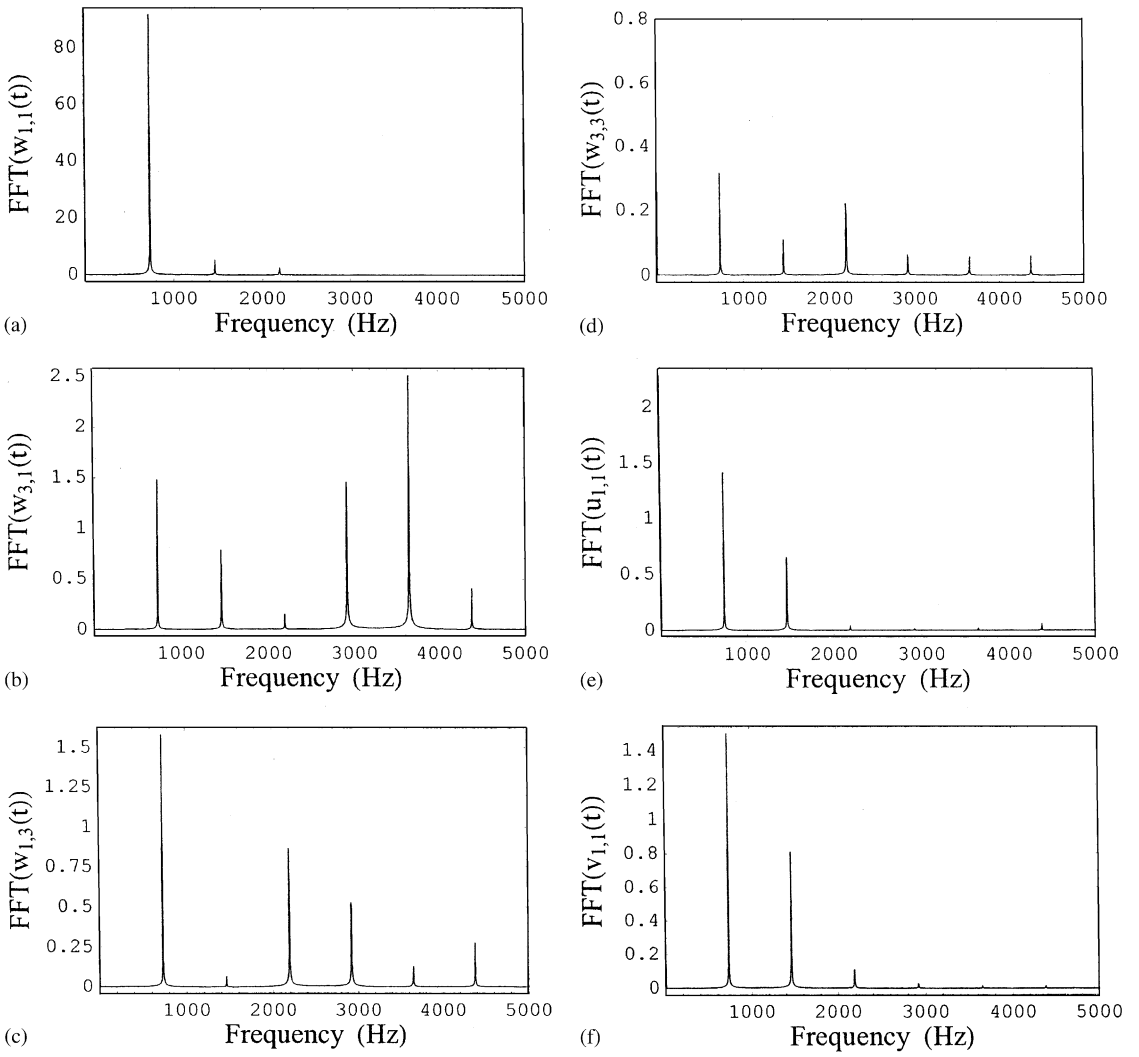

Fig. 11. Spectrum of the response of the panel; excitation frequency $\omega = 1.1\ \omega_{1,1}, \tilde{f} = 10.68$ N and $\zeta_{1,1} = 0.004$; 16 dofs. (a) Generalized coordinate $w_{1,1}$; (b) generalized coordinate $w_{3,1}$; (c) generalized coordinate $w_{1,3}$; (d) generalized coordinate $w_{3,3}$; (e) generalized coordinate $u_{1,1}$; (f) generalized coordinate $v_{1,1}$.

have been obtained by using the simplified Eqs. (24b, 25b). In particular, the amplitude of the generalized coordinates $w_{3,1}$ and $w_{1,3}$ is largely increased (about two times with respect to Fig. 6b, c). A main internal resonance arises for excitation frequency $\omega = 1.03\ \omega_{1,1}$; this is associated with a peak in the response of both $w_{1,3}$ and $w_{3,3}$ and is a non-periodic combination resonance [24], in particular $3(1.03\omega_{1,1}) = \omega_{3,3} - \omega_{1,3}$. A second internal resonance arises for excitation frequency $\omega \approx 1.18\ \omega_{1,1}$ and could be due to $2(1.18\omega_{1,1}) = 2\omega_{3,3} - 3\omega_{1,3}$. However, it is extremely close also to $3\ (1.223\ \omega_{1,1}) = 2\omega_{1,3} - \omega_{3,1}$ and to $3\ (1.279\ \omega_{1,1}) = \omega_{1,3}$, so a much more complex interaction of modes is also possible.

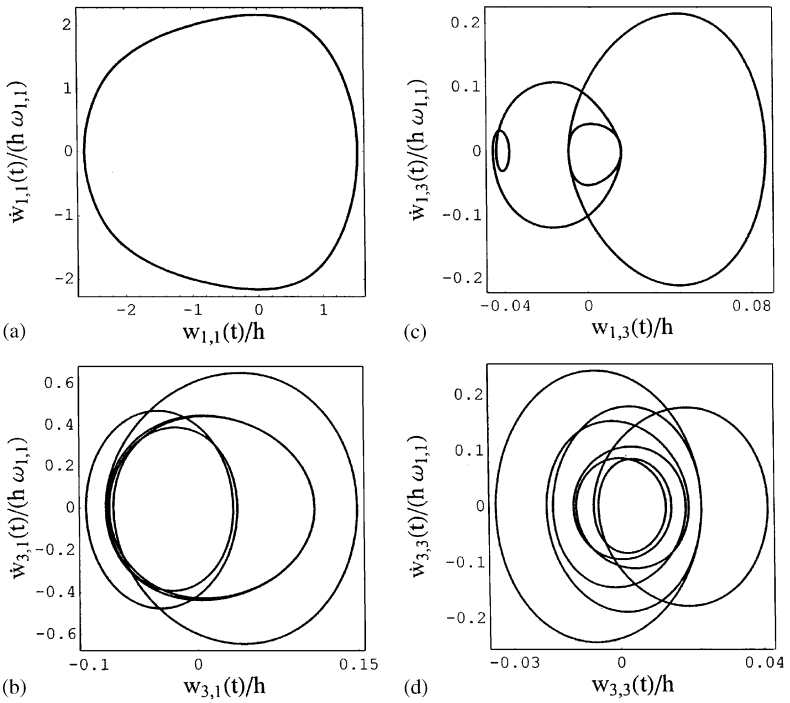

Fig. 12. Phase plane diagram of the panel; excitation frequency $\omega = 1.1\,\omega_{1,1}$, $\tilde{f} = 10.68$ N and $\zeta_{1,1} = 0.004$; 16 dofs. (a) Generalized coordinate $w_{1,1}$; (b) generalized coordinate $w_{3,1}$; (c) generalized coordinate $w_{1,3}$; (d) generalized coordinate $w_{3,3}$.

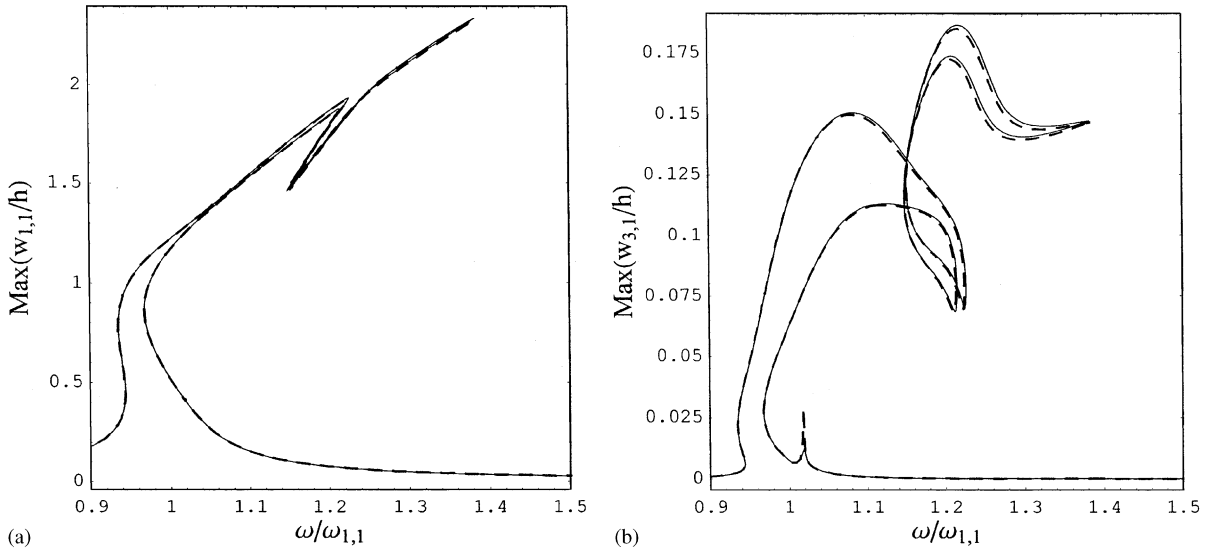

Fig. 13. Maximum amplitude of the panel response versus the excitation frequency calculated by using two different shell theories; mode ($m = 1$, $n = 1$), $\tilde{f} = 10.68$ N and $\zeta_{1,1} = 0.004$; 16 dofs. - -, Novozhilov's theory; —, Donnell's theory. (a) Generalized coordinate $w_{1,1}$; (b) generalized coordinate $w_{3,1}$.

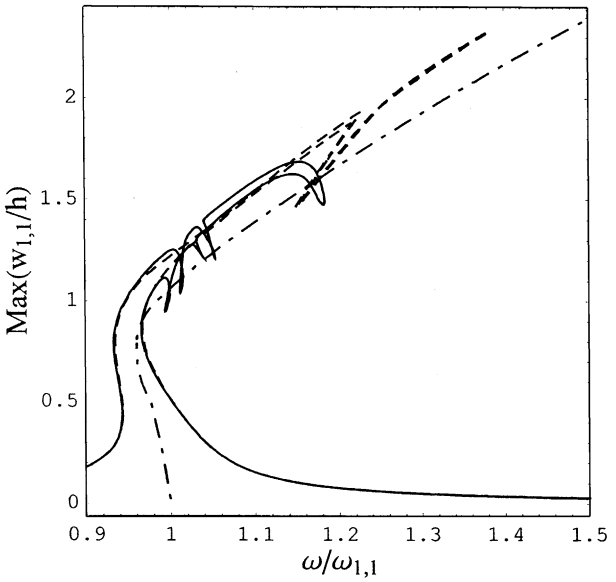

Fig. 14. Maximum amplitude of the radial response of the panel (generalized coordinate $w_{1,1}$) versus the excitation frequency; fundamental mode ($m = 1$, $n = 1$), $\tilde{f} = 10.68$ N and $\zeta_{1,1} = 0.004$; Donnell's theory. —, present results, 24 dofs with Eqs. (24a, 25a); - -, present results, 9 dofs; – - – , backbone curve from Kobayashi and Leissa [13].

6. Conclusions

The present study introduces a multimode expansion and uses accurate shell theories retaining in-plane inertia to study large-amplitude, forced vibrations of circular cylindrical panels. This overcomes two frequent limitations in previous studies: (i) the use of mode expansions with one or 2 dofs; and (ii) the use of less accurate, but simpler, Donnell's shallow-shell theory.

The occurrence of some internal resonances in the problem studied is a clear indication that this important nonlinear phenomenon has fundamental importance in the study of curved panels. Internal resonances can be studied only with multimode expansions, in some cases with a quite large number of dofs.

A comparison of large-amplitude vibrations of circular cylindrical panels and circular cylindrical shells, complete around the circumference, shows that panels have a much stronger nonlinearity than complete shells; this nonlinearity is initially of the softening type, turning to hardening for vibration amplitude outwards around the panel thickness. Differently, complete shells display initial weak softening type behaviour with a smaller change in frequency and turn to hardening behaviour for larger vibration amplitude; moreover, they present travelling waves at resonance due to the axial symmetry.

Acknowledgement

This work was partially supported by the FIRB 2001 grant of the Italian Ministry for University and Research (MIUR).

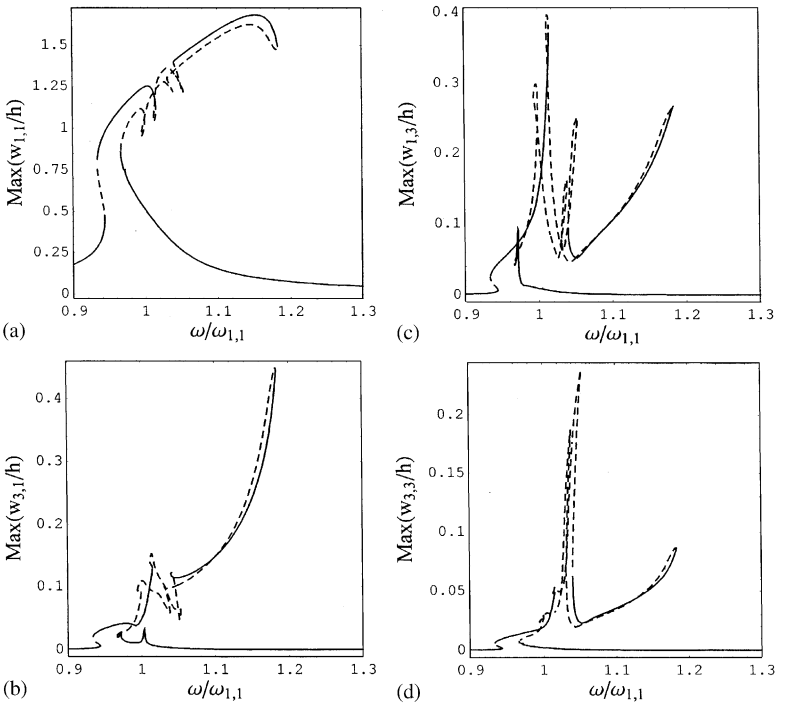

Fig. 15. Maximum amplitude of the response of the panel versus the excitation frequency with stability indication; 24 dofs with Eqs. (24a, 25a), fundamental mode ($m = 1$, $n = 1$), $\tilde{f} = 10.68$ N and $\zeta_{1,1} = 0.004$; Donnell's theory. —, stable solution; - -, unstable solution. (a) Generalized coordinate $w_{1,1}$; (b) $w_{3,1}$; (c) $w_{1,3}$; (d) $w_{3,3}$.

References

[1] M. Amabili, M.P. Païdoussis, Review of studies on geometrically nonlinear vibrations and dynamics of circular cylindrical shells and panels, with and without fluid–structure interaction, *Applied Mechanics Reviews* 56 (2003) 349–381.

[2] E. Reissner, Nonlinear effects in vibrations of cylindrical shells, Ramo-Wooldridge Corporation Report AM5-6 1955.

[3] E.I. Grigolyuk, Vibrations of circular cylindrical panels subjected to finite deflections, *Prikladnaya Matematika i Mekhanika* 19 (1955) 376–382 (in Russian).

[4] B.E. Cummings, Large-amplitude vibration and response of curved panels, *AIAA Journal* 2 (1964) 709–716.

[5] A.W. Leissa, A.S. Kadi, Curvature effects on shallow shell vibrations, *Journal of Sound and Vibration* 16 (1971) 173–187.

[6] A.S. Vol'mir, A.A. Logvinskaya, V.V. Rogalevich, Nonlinear natural vibrations of rectangular plates and cylindrical panels, *Soviet Physics — Doklady* 17 (1973) 720–721.

[7] D. Hui, Influence of geometric imperfections and in-plane constraints on nonlinear vibrations of simply supported cylindrical panels, *Journal of Applied Mechanics* 51 (1984) 383–390.

[8] L. Librescu, M.-Y. Chang, Effects of geometric imperfections on vibration of compressed shear deformable laminated composite curved panels, *Acta Mechanica* 96 (1993) 203–224.

[9] C.Y. Chia, Nonlinear analysis of doubly curved symmetrically laminated shallow shells with rectangular platform, *Ingenieur-Archiv* 58 (1988) 252–264.

[10] Y.M. Fu, C.Y. Chia, Multi-mode non-linear vibration and postbuckling of anti-symmetric imperfect angle-ply cylindrical thick panels, *International Journal of Non-Linear Mechanics* 24 (1989) 365–381.
[11] R.A. Raouf, A qualitative analysis of the nonlinear dynamic characteristics of curved orthotropic panels, *Composites Engineering* 3 (1993) 1101–1110.
[12] R.A. Raouf, A.N. Palazotto, On the non-linear free vibrations of curved orthotropic panels, *International Journal of Non-Linear Mechanics* 29 (1994) 507–514.
[13] Y. Kobayashi, A.W. Leissa, Large amplitude free vibration of thick shallow shells supported by shear diaphragms, *International Journal of Non-Linear Mechanics* 30 (1995) 57–66.
[14] T. Yamaguchi, K. Nagai, Chaotic vibration of a cylindrical shell-panel with an in-plane elastic-support at boundary, *Nonlinear Dynamics* 13 (1997) 259–277.
[15] T. Yamaguchi, K. Nagai, Chaotic oscillations of a shallow cylindrical shell-panel with a concentrated elastic-support in: M.P. Païdoussis, M. Amabili, P.B. Gonçalves, (Eds.), *Nonlinear Dynamics of Shells and Plates*, AMD, Vol. 238, ASME, New York, 2000, pp. 85–94.
[16] A.A. Popov, J.M.T. Thompson, J.G.A. Croll, Bifurcation analyses in the parametrically excited vibrations of cylindrical panels, *Nonlinear Dynamics* 17 (1998) 205–225.
[17] A. Abe, Y. Kobayashi, G. Yamada, Non-linear vibration characteristics of clamped laminated shallow shells, *Journal of Sound and Vibration* 234 (2000) 405–426.
[18] M. Amabili, M. Pellegrini, M. Tommesani, Experiments on large-amplitude vibrations of a circular cylindrical panel, *Journal of Sound and Vibration* 260 (2003) 537–547.
[19] M. Amabili, Comparison of shell theories for large-amplitude vibrations of circular cylindrical shells: Lagrangian approach, *Journal of Sound and Vibration* 264 (2003) 1091–1125.
[20] N. Yamaki, *Elastic Stability of Circular Cylindrical Shells*, North-Holland, Amsterdam, 1984.
[21] A. W. Leissa, *Vibration of Shells*, NASA SP-288, Government Printing Office, Washington, DC, 1973. Now available from, The Acoustical Society of America 1993.
[22] S. Wolfram, *The Mathematica Book*, fourth ed., Cambridge University Press, Cambridge, UK, 1999.
[23] E.J. Doedel, A.R. Champneys, T.F. Fairgrieve, Y.A. Kuznetsov, B. Sandstede, X. Wang, AUTO 97, continuation and bifurcation software for ordinary differential equations (with HomCont), Concordia University, Montreal, Canada, 1998.
[24] G. Schmidt, A. Tondl, *Non-Linear Vibrations*, Cambridge University Press, Cambridge, UK, 1986.